Springer

Journal of Mechanical Science and Technology 23 (2009) 1342~1353

Journal of Mechanical Science and Technology

www.springerlink.com/content/1738-494x
DOI 10.1007/s12206-009-0353-0

ExLO: A three-dimensional total shock physics FEM code †

Minhyung Lee[1,*], Wan-Jin Chung[2], Hak Jun Kim[3] and Hyung Won Kim[3]

[1]*Department of Mechanical Engineering, Sejong University, 98 Kunja-Dong, Kwang-Jin Gu, Seoul, 143-747 Korea*
[2]*Department of Die & Mould Engineering, Seoul National University of Technology, Seoul, 139-737 Korea*
[3]*Agency for Defense Development, Jochiwongil 462, Yuseong, Daejeon, Korea*

(Manuscript Received February 22, 2008; Revised March 10, 2009; Accepted March 10, 2009)

Abstract

A unified shock physics code, ExLO, in which Lagrangian, ALE and Eulerian solvers are incorporated into a single framework, has recently been developed in Korea. It is based on the three-dimensional explicit finite element method and written in C++. ExLO is mainly designed for the calculation of structural responses to highly transient loading conditions, such as high-speed impacts, high-speed machining and explosions. In this paper the numerical schemes are described. Some improvements of the material interface and advection scheme are included. Details and issues of the momentum advection scheme are provided. Numerical predictions are in good agreement with the existing experimental data. Specific applications of the code are discussed in a separate paper in this journal. Eventually, ExLO will provide an optimum simulation environment to engineering problems including the fluid-structure interaction problems, since it allows regions of a problem to be modeled with Lagrangian, ALE or Eulerian schemes in a single framework.

Keywords: ExLO; Eulerian; FEM; Impact; Explosion

1. Introduction

Understanding and controlling large plastic deformation problems such as high-speed impact/penetration and explosion events are of great importance due to their practical applications. Hydrocodes (or wavecode) based on continuum mechanics solve such a highly dynamic events. The Lagrangian, Eulerian and ALE (arbitrary Lagrangian-Eulerian) schemes were developed in the early sixties. Recently, an explicit dynamic FE-code has become an excellent analysis tool for large-scale structural simulations in the research labs [1, 2], universities [3-5] and industrial companies [6, 7] as well. For large-scale simulation and enhanced accuracy, more advances in the fields of parallelization [8] and adaptive meshing [9] have been made since the late nineties.

The study presented in this paper represents a recent effort in Korea to develop a three-dimensional explicit program of unified Lagrangian, ALE and Eulerian schemes for the purpose of providing an optimum simulation environment in a single code framework, ExLO [10]. Three-dimensional eight node brick element is used with one point integration scheme to prevent locking. ExLO has several models that are useful for simulating strong shocks of large deformation events. Currently elastic-plastic behavior, Johnson-Cook fracture model and null model are available. Several equations of state (EOS), such as the Jones-Wilkins-Lee (JWL) for high explosive reactive products, the ideal gas, and Mie-Grunisen type can be chosen. It uses second-order advection schemes between cells. Some details of schemes used in the Lagrangian part, the remap part and how the interface between each parts are fully described in this paper.

The main code structure indicating major calculation phases is stated in Section 2. Then the schemes of

† This paper was recommended for publication in revised form by Associate Editor Heoung Jae Chun

*Corresponding author. Tel.: +82 2 3408 3282, Fax.: +82 2 3408 4333
E-mail address: mlee@sejong.ac.kr

© KSME & Springer 2009

each calculation phase follow. The Lagrangian step is briefly discussed in Section 3 with validation for the Taylor bar impact test. The remap is included in Section 4. Some issues in this part are added and discussed in detail. The specific application of ExLO for the high-speed impact/penetration and explosion events involving large plastic deformations is described in a separate paper in this journal.

2. Unified code structure

2.1 Eulerian mesh and variable positions

Three-dimensional rectangular meshes using three sets of spatial coordinates x (i), y (j) and z (k) are currently available as shown in Fig. 1. Each computational element is a box. One-dimensional and two-dimensional simulations can also be modeled by using wedged-shaped 8 node elements. Except the nodal velocities, all other variables, such as the stress, density and internal energy, are cell-centered. The major advection algorithm is thus constructed from the cell-centered algorithm. The advection algorithm for momentum is also based on the cell-centered algorithm. Nodal mass is one-eighth the mass of the eight surrounding elements.

2.2 Operator-splitting

We split a time step into two parts: Lagrangian and remap parts. The first part, Lagrangian step, calculates the incremental motion of material and is actually the same with the generic Lagrangian code. The second part, called remap step or advection step, solves the transport of material properties between mesh cells. If we include some generosity of the node movement (remesh step) between two parts, actually ALE calculation can be conducted as shown in Fig. 2. The governing equation in the general conservation form is,

$$\frac{\partial \phi}{\partial t} + \nabla \cdot \Phi = S \,, \tag{1}$$

where ϕ is a solution vector, Φ a flux function, and S a source term. This equation can be split as [1, 11],

$$\frac{\partial \phi}{\partial t} = S \,, \text{ Lagrangian step} \tag{2a}$$

$$\frac{\partial \phi}{\partial t} + \nabla \cdot \Phi = 0 \,, \text{ Remap step} \tag{2b}$$

2.3 Interface of lagrangian part and remap part

The flowchart of the ExLO solution algorithm is presented in Fig. 3. As discussed in the previous section, the algorithm is separated into mainly three sections. First, an initialization process is done by using an input file. All the vertex and cell-centered quantities are initialized. The code now advances to the next time step to calculate the Lagrangian deformations. It is important to note that a mixture theory, which is not present in the ordinary explicit Lagrangian code, is necessary to calculate the mean stress of a mixed cell. The pressure calculation using the equation of state and energy equation is followed.

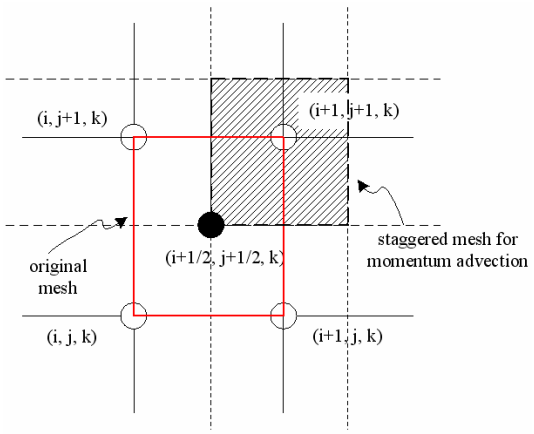

Fig. 1. ALE/Eulerian mesh system.

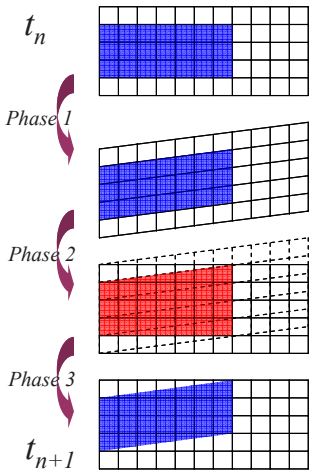

Fig. 2. Code structure in a single framework, (a) phase 1: Lagrangian step, (b) phase 2: Remesh step, (c) Remap step.

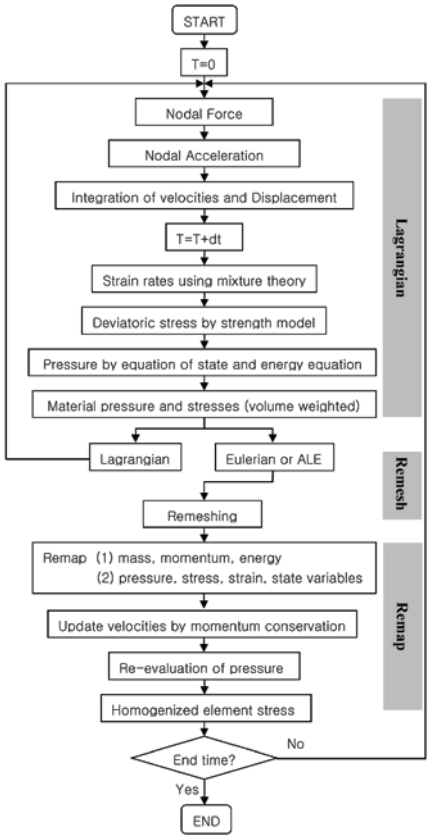

Fig. 3. A general flow-chart for the ExLO code.

The mesh shape can also be modified depending on the type of calculation. In the purely Lagrangian case, no modification is made and the computaion cyle is completed. In the ALE case new grid coordinates are computed by using several options on the movement restriction, while in the Eulerian case the vertex moves back to the original location. For both cases the new cell volume and the vertex velocities are calculated. The remeshing process involves advection of the cell-centered properties, such as density and internal energy. The vertex-centered momentum is also advected by using a similar method of cell-centered advection. After advection the equation of state is reapplied to update the pressure by using the new cell density and new cell energy.

3. Lagrangian step

3.1 Mathematical formulation

A three-dimensional eight node brick element is used and one point integration scheme is applied to prevent locking. Spurious modes due to lack of integration points are controlled by hourglass control [12]. In practice it is also true that the one point integrated element has a reliability problem and hourglass control needs to be selected with great care [13]. Velocities **u** and coordinates **x** are updated with the half step central difference method,

$$\mathbf{u}^{n+1/2} = \mathbf{u}^{n-1/2} + \Delta t^n \ddot{\mathbf{u}}^n , \tag{3}$$

$$\mathbf{x}^{n+1} = \mathbf{x}^n + \Delta t^{n+1/2} \mathbf{u}^{n+1/2} , \tag{4}$$

$$\Delta t^n = \frac{\left(\Delta t^{n-1/2} + \Delta t^{n+1/2}\right)}{2} , \tag{5}$$

where the superscript (n) indicates the time step. The accelerations are determined by using the diagonal mass matrix **M** as,

$$\dot{u} = \frac{1}{\mathbf{M}} \left(F^{ext} - \int \mathbf{B}^T \bar{\sigma} d\Omega \right), \tag{6}$$

where **B** is the discrete gradient operator. In the explicit Lagrangian step used in the multi-material Eulerian code, $\bar{\sigma}$ is the mean stress and is calculated according to mixture theory.

3.2 Equation of state (EOS) and energy equation

The equation of state and energy equation are solved simultaneously for the hydrostatic pressure P and internal energy e as follows.

$$P = f(\rho, e), \tag{7}$$

$$e^{n+1} = e^n + \Delta e_d^{\,n+1/2} - \left[\frac{P^{n+1} + P^n}{2} + q^{n+1/2} \right] \frac{\Delta V^{n+1}}{m_c} , \tag{8}$$

where e_d is the distortional energy and m_c the cell mass. For example, the two equations for air medium are,

$$P^{n+1} = (\gamma - 1) \rho^{n+1} e^{n+1} , \tag{9}$$

$$e^{n+1} = e^n - \left[\frac{P^{n+1} + P^n}{2} + q^{n+1/2} \right] \frac{\Delta V^{n+1}}{m_c} , \tag{10}$$

where γ (=1.4) is the ratio of specific heats and a gamma law equation of state is used. Substituting Eq. (9) into Eq. (10) and solving for new energy results in,

$$e^{n+1} = \frac{\left[e^n - \left(\frac{P^n}{2} - q^{n+1/2} \right) \frac{\Delta V^{n+1}}{m_c} \right]}{\left[1 + \frac{(\gamma - 1)\Delta V^{n+1}}{2m_c} \rho^{n+1} \right]}. \quad (11)$$

3.3 Constitutive equations

The stresses in the material are expressed as the sum of the dilatational and deviatoric parts s_{ij} as,

$$\sigma_{ij} = -P\delta_{ij} + s_{ij} \ , \quad (12)$$

The dilatational response is governed by an equation of state and the deviatoric response by a plasticity flow theory. For objective stress update the Jaumann rate is used as,

$$\hat{s}_{ij} = \dot{s}_{ij} + s_{ik}\Omega_{kj} - \Omega_{ik}s_{kj} \ , \quad (13)$$

where $\dot{s}_{ij}$ is the derivative of s_{ij}. Ω_{ij} is the rigid body rotation (spin) tensor which is,

$$\Omega_{ij} = \frac{1}{2}\left(\frac{\partial u_i}{\partial x_j} + \frac{\partial u_j}{\partial x_i} \right). \quad (14)$$

Constitutive models adopted in the code are von Mises type and the Johnson-Cook viscoplastic models. The flow stresses are in general form,

$$\sigma_y = \left[A + B\varepsilon_p^n \right], \quad (15)$$

$$\sigma_y = \left[A + B\varepsilon_p^n \right] \left[1 + C\ln\dot{\varepsilon}^* \right] \left\{ 1 - \left[\frac{T - T_o}{T_{melt} - T_o} \right]^m \right\}, \quad (16)$$

where ε is the equivalent plastic strain, $\dot{\varepsilon}^*$ the dimensionless plastic strain rate and T the temperature. T_{melt} and T_o are the melting and reference temperatures.

To handle the discontinuity in the flow variables associated with shocks, it has been a common practice to introduce an extra viscous term. Hence the artificial bulk viscous terms are added to the hydrostatic pressure. The actual terms, which are added to the hydrostatic pressure in the current program, are

$$q = \begin{cases} \rho_0 L_e \left(b_0 L_e \dot{\varepsilon}_{kk}^{\ 2} - b_1 c \dot{\varepsilon}_{kk} \right) & for \ \ \dot{\varepsilon}_{kk} < 0 \\ 0 & for \ \ \dot{\varepsilon}_{kk} \geq 0 \end{cases}, \quad (17)$$

where ρ_o is the reference density, L_e the characteristic length and $\dot{\varepsilon}_{kk}$ the volume change, c the wave speed. b_o and b_1 are the coefficients in the bulk viscosity, and typically $b_o = 1.5$ and $b_1 = 0.06$. The critical time step for stability is determined to meet the CFL condition.

3.4 Taylor bar benchmark test

Since the program runs as a pure Lagrangian code by skipping the remap part, the Lagrangian part has been tested for the well known Taylor bar benchmark problem. The results are compared with experimental data [14]. A cylindrical rod impacts against a rigid wall at velocities of 219 *m*/*s* for Al 7075-T6 rod and 145 *m*/*s* for OHFC copper rod, as shown in Fig. 4. The von Mises material model is used. The yield strength is 700 MPa for AL 7075-T6, and 350 MPa for OHFC copper, respectively. Fig. 5 shows a comparison of ExLO predictions and experimental data for final deformed shape at a sufficient time after impact, indicating a good match. The dotted line is the deformed shape from experiment. A good agreement is also predicted for OHFC copper rod, as shown in Fig. 6. The numerical results for final rod length and deformed diameter are compared with experimental data from open literature in Table 1. The results are reasonably comparable. A little discrepancy might be due to the material properties, which may not be perfectly described by the von Mises strength model. Up to here validation of the Lagrangian step has been performed.

At the end of the Lagrangian computational step and before the remap step, it is necessary to include

Table 1. Comparison of the final diameter and final length of the rod.

	AL 7075-T6		OHFC Copper	
	ExLO	Experiment	ExLO	Experiment
Impact Velocity (m/s)	219		145	
Initial Diameter (mm) / Inital Length of the Rod (mm)	4.16 / 31.2		4.16 / 31.4	
Deformed Diameter (mm)	5.36	5.02	7.14	6.36
Final Length of the Rod (mm)	28.87	28.65	25.40	25.80

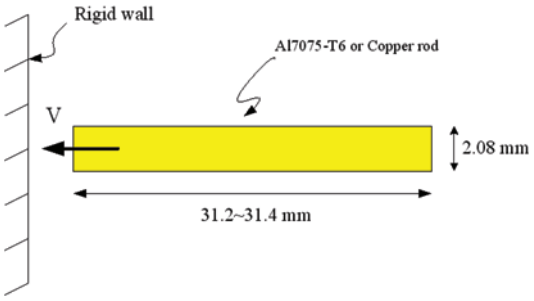

Fig. 4. Schematic of Taylor bar benchmark test.

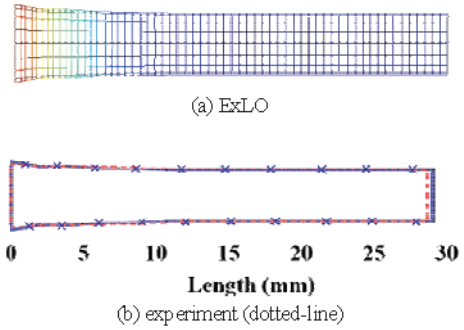

Fig. 5. Taylor bar impact of Al7075-T6, impact velocity 219 m/s.

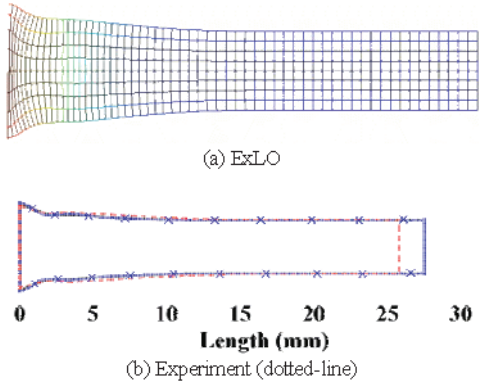

Fig. 6. Taylor bar impact of OHFC copper, impact velocity 145 m/s.

an additional step in which grid motion is controlled. This is called as "remesh step". Various options for the grid motion will be predescribed. One of them is a Eulerian fixed grid, which constrains the node to move back to the original positions.

4. Remap step

The remesh step associates advection of element properties. The major processes of the remap step are the calculation of volume flux, material interface tracking, advection of cell-centered variables and advection of vertex-centered variables. For the material interface tracking, ExLO uses the SLIC-like algorithm with an enhancement to account for some special topologies. Youngs' 2nd order algorithm is under investigation. In some aspect, the benefit of using a sophisticated algorithm such as the three dimensional Youngs' algorithm is somewhat less since the scheme is quite complex and takes more computational time.

The advection equations are simplified by using operating splitting techniques, such that the three-dimensional governing equations are replaced by a set of one-dimensional equations. ExLO uses the Youngs' 2nd order accurate scheme with the van Leer scheme to preserve monotonicity. Finally, for the vertex-centered advection such as nodal momentum, the SALE algorithm, which is simple and easy to implement, is adopted and some modifications are being investigated. More details and modifications for the schemes used in the remap part are described below.

4.1 Interface tracking schemes

In the present work a VOF (Volume of Fluid) based method is used to capture the moving boundaries in a 3-Dim, rectangular-grid system. The method is applicable to the type of code in which the layout of materials is described solely by the volume fraction of the various materials in each computational cell. The volume fraction distribution is used to construct an interface in each mixed cell by a line in two-dimensional mesh and a plane in three-dimensional mesh. The position of the interface determines the flow across cell sides and hence enables volume fractions to be updated to the next time level. Currently, the 1st order scheme is well implemented and the 2nd order scheme is still under fine refinement.

The evolution of material interfaces is determined by the following equation:

$$\sum_{m=1}^{N}\left\{\frac{\partial f^m}{\partial t}+u\cdot\nabla f^m\right\}=0\,, \tag{18}$$

where N is the total number of materials, u the fluid velocity, and $f^m(=V_m/V)$ the volume of fraction of the mth fluid material. If the cell is empty of material m, $f^m=0$. Hence the volume fraction is advected with

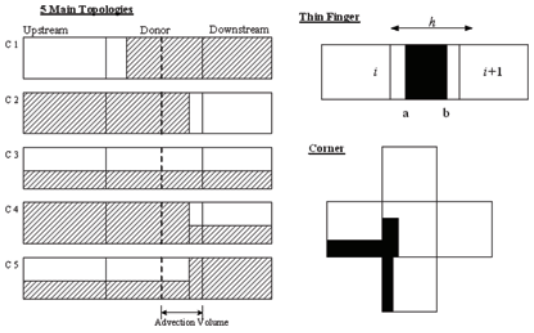

Fig. 7. Five fluid volume topologies and special cases.

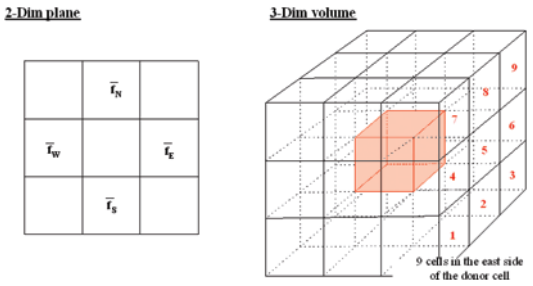

Fig. 8. Difference stencil for the weighted average of the volume fractions.

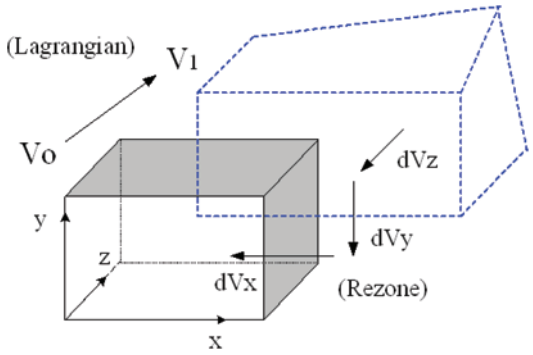

Fig. 9. Volume fraction update by volume rezone with alternating sweeps in each direction.

the flow characteristics of the system.

Most popular and simple method in this category is SLIC (simple line interface construct) developed by [15]. The interface is constructed by using adjacent elements in a row and column of elements without using information in the transverse mesh direction. Hence, the interface surface is aligned either parallel or perpendicular to the flow vector in each sweep direction, which may cause an inaccuracy for off-axis translational flows. This is why this belongs to a *piecewise-constant method*. To predict more accurate interfaces, while keeping the simplicity of the philosophy of the methodology, a modifed SLIC-like algorithm [16] is currently implemented. However, the results were not fully successful and more cases are required, such as "thin finger" and "corner" topologies (see Fig. 7).

Piecewise-linear methods calculate the interface lines (2-Dim) and planes (3-Dim) with slope. Among them, the two-dimensional Youngs' scheme has been known to predict accurate interfaces [17], although the three-dimensional methodology is not simple. Here the major idea of the scheme is provided briefly. First, it is necessary to determine interface normal direction by using volume fraction information from the surrounding cells. Using a stencil for a mesh, the normal is determined as,

$$\bar{n} = -\frac{\nabla f}{|\nabla f|}, \qquad \frac{\partial f}{\partial x} = \frac{\bar{f}_E - \bar{f}_W}{2\Delta x}, \quad \frac{\partial f}{\partial y} = \frac{\bar{f}_N - \bar{f}_S}{2\Delta y}, \quad \frac{\partial f}{\partial z} = \frac{\bar{f}_F - \bar{f}_B}{2\Delta z}. \tag{19}$$

This indicates that components of the volume fraction gradient are determined from the weighted averages of the volume fractions as shown in Fig. 8. There are several ways to determine the weighted averages. The one of $\bar{f}_E(i+1,j,k)$ is,

$$\bar{f}_E = -\frac{\{(f_1+f_3+f_7+f_9)+\beta(f_2+f_2+f_4+f_6)+\gamma(f_5)\}}{(4+4\beta+\gamma)}, \tag{20}$$

where $\beta = 2$ and $\gamma = 4$. Next, the interface position is adjusted to match the volume fraction of the donor cell. The procedure is much simplified by transforming to a unit cube co-ordinate system. There are six cases of the shape formed from the intersections of the cube with an arbitrary plane [18, 19]. The distance from the cube origin to the plane can be expressed as a function of the interface normal and volume fraction.

Once the location of the interface is determined, the portion of flux corresponding to the fluid under consideration needs to be calculated. First, the exit face has to be identified and a plane is drawn parallel to the exit face. Then the exit volume between the two planes and within the fluid is estimated. This volume flux and the fluid volume flowing with it are used to update the volume fraction every time step. Fig. 9 illustrates the updating procedure: (1) the cell volume

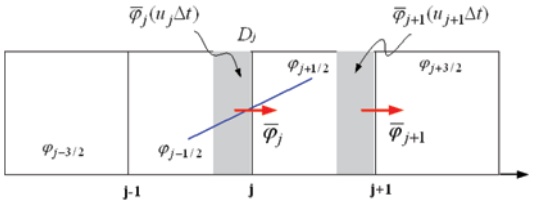

Fig. 10. Material property indices in cell centered ($j \pm 1/2$) and cell boundary (j), the property gradient (D_j) is defined at the cell boundary.

changes from V_o to V_1 in the Lagrangian step while the volume fraction remains constant, (2) the vertex moves back to the Eulerian original location, (3) the volume fraction advection is carried out in each direction one by one with alternating sweeping direction every other step.

4.2 Cell-centered advection

Since spatial operating splitting is applicable, the following one-dimensional advection equation can be applied to three-dimensional problems [18].

$$\frac{\partial \varphi}{\partial t} + u\frac{\partial \varphi}{\partial x} = 0. \tag{21}$$

The discrete form of this equation is,

$$\varphi^{+}_{j+1/2} = \varphi^{-}_{j+1/2} + \frac{\left(\overline{\varphi}_j u_j - \overline{\varphi}_{j+1} u_{j+1}\right)}{\Delta x}\Delta t\ , \tag{22}$$

where $\overline{\varphi}$ is the average value of the flowing property and the notations are illustrated in Fig. 10. The superscripts (+) and (−) indicate the values before and after the advection, respectively. Note that no time step is involved in the remap part. If we take into account a linear variation of the cell property, it can be expressed as a spatial variation function,

$$\varphi(x) = \varphi_{j-1/2} + D_j x\ , \tag{23}$$

where D_j is the slope at the cell boundary. The average value of the flowing property is then given by,

$$\overline{\varphi}_j = \begin{cases} \varphi_{j-1/2} + \dfrac{1}{2}\left(1 - \dfrac{u\Delta t}{\Delta x}\right)D_j x, & u > 0 \\ \varphi_{j+1/2} - \dfrac{1}{2}\left(1 + \dfrac{u\Delta t}{\Delta x}\right)D_j x, & u < 0 \end{cases}, \tag{24}$$

where,

$$D_j = \begin{cases} 0 & \text{1st order (upwind method)} \\ \dfrac{\varphi_{j+1/2} - \varphi_{j-1/2}}{\Delta x} & \text{2nd order} \end{cases} \tag{25}$$

The above one-dimensional advection formulations are to be applied to each x, y and z direction. The order used is x-y-z and z-y-x on alternate time steps to prevent systematic error. Numerical diffusion associated with the 1st-order advection can be eliminated by using the 2nd-order equation. However some non-physical oscillations and negative properties may be observed and this can be manipulated by the monotonic advection method of van Leer, which is often referred to as the MUSCL algorithm [20].

4.3 Vertex-centered advection

The momentum advection takes advantage of the cell-centered advection method already discussed previously. The one-dimensional concept is first discussed and followed by the two-dimensional extension. During the extension to the two-dimensional model, some aspects that are not present in one-dimension are included here. Inclusion of the three-dimensional formulation in this paper seems to be redundant.

The basic idea is that the change in the momentum of a node is an algebraic average of the changes in the momentum of its surrounding cells [21]. For the one-dimensional case, we need to define the cell momentum and nodal momentum using the cell mass $m_{j+1/2}$ and nodal mass m_j as,

$$M_{j+1/2} = \tfrac{1}{2} m_{j+1/2}\left(u_j + u_{j+1}\right)\text{: cell momentum,} \tag{26}$$

$$M_j = m_j u_j \ \text{: nodal momentum.} \tag{27}$$

The updated nodal momentum is obtained from the change in the cell momentum $\Delta M_{j\pm1/2}$ from the advection as,

$$M^{+}_j = M^{-}_j + \frac{1}{2}\left(\Delta M_{j-1/2} + \Delta M_{j+1/2}\right), \tag{28}$$

where again the superscripts (+) and (−) indicate the values before and after the advection, respectively. Finally the updated nodal velocity is,

$$u_j^+ = \frac{M_j^+}{m_j^+}. \tag{29}$$

For the two-dimensional case as shown in Fig. 11, each cell has two momentum components in each direction (k, l) and they are written using the cell mass by,

$$\begin{aligned} Mx_{(k+1/2,l+1/2)} &= \tfrac{1}{4} m_{(k+1/2,l+1/2)} \\ &\quad \left(u_{(k,l)} + u_{(k+1,l)} + u_{(k,l+1)} + u_{(k+1,l+1)}\right) \\ My_{(k+1/2,l+1/2)} &= \tfrac{1}{4} m_{(k+1/2,l+1/2)} \\ &\quad \left(v_{(k,l)} + v_{(k+1,l)} + v_{(k,l+1)} + v_{(k+1,l+1)}\right) \end{aligned}. \tag{30}$$

Again, the updating of each component of the nodal momentum is obtained from the change in the cell momentum ΔMx and ΔMy from the advection in each direction as,

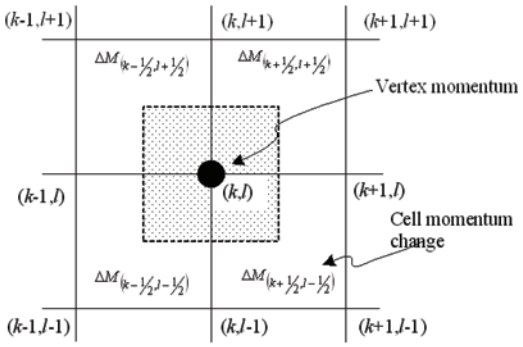

(a)

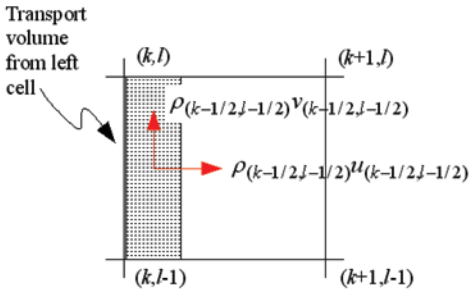

(b)

Fig. 11. (a) Vertex momentum is obtained as one quarter of the sum of the changes in the momentum of four surrounding cells in 2-Dim and one-eighth of eight surrounding cells in 3-Dim. (b) Each component of momentum associated with the transport volume is advected.

$$\begin{aligned} Mx^+_{(k,l)} &= Mx^-_{(k,l)} + \frac{1}{4}(\Delta Mx_{(k-1/2,j-1/2} + \Delta Mx_{(k+/12,j-1/2)} \\ &\quad + \Delta Mx_{(k-1/2,j-1/2} + \Delta Mx_{(k+/12,j-1/2)}), \\ My^+_{(k,l)} &= My^-_{(k,l)} + \frac{1}{4}(\Delta My_{(k-1/2,j-1/2} + \Delta My_{(k+/12,j-1/2)} \\ &\quad + \Delta My_{(k-1/2,j-1/2} + \Delta My_{(k+/12,j-1/2)}). \end{aligned} \tag{31}$$

That is, the x and y components of the velocity are advected in an identical manner. Finally, for the updated nodal velocities, Eq. (29) is still applicable here and even to the three-dimensional formulations.

Now we need to pay special attention to the calculation of the change in the cell momentum, ΔMx and ΔMy. For the one-dimensional case and $u > 0$, $\Delta M_{j+1/2}$ is simply,

$$\Delta M_{j+1/2} = (\rho_{j-1/2} u_{j-1/2})\Delta V_j - (\rho_{j+1/2} u_{j+1/2})\Delta V_{j+1}, \tag{32}$$

where $(\rho_{j-1/2} u_{j-1/2})$ is the specific momentum of $(j-1/2)$ cell and this equation means that the change in the momentum of $(j+1/2)$ cell is obtained from the difference between the incoming momentum from $(j-1/2)$ cell through the cell boundary j and the outgoing momentum through the cell boundary $j+1$. ΔV_j is the transport volume through the cell boundary j and is determined from the interface tracking scheme described previously. That is, for the one-dimensional case only x-momentum is associated with the transport volume. For the two-dimensional case, however, the transport volume associates two momentum components to be advected as illustrated in Fig. 11. It is true for the three-dimensional case as well.

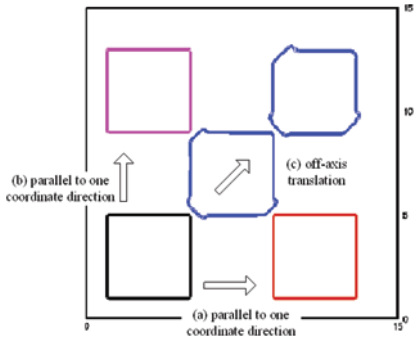

Fig. 12. Advection of the square volume with unidirectional velocity field. At the bottom left are the initial conditions (I.C.). The top left and bottom right are the advection with parallel to one axis direction. The center and the top right is the advection with off-axis direction.

In the current work the cell-centered advection is a second-order scheme. In transport of the momentum in Eq. (32), an average density estimated form the second-order scheme is used. However, the velocity is assumed to be a piecewise-constant distribution. We leave a piecewise-linear distribution for momentum to future work.

4.4 Simple advection test

In this section the remap part is tested with simple analytic velocity fields, in which no stresses are involved. Three different velocity fields are considered: (1,0), (0,1) and (1,1). The computational domain is 150 × 150 × 1 mesh cells. The initial conditions are a square volume filled with 20 × 20 × 1 cells at the left bottom of the figure.

The results of advecting the scalar field with the three velocity fields are shown in Fig. 12(a) for (1,0), (b) for (0,1), and (c) for (1,1) velocity fields. The results are displayed on the same figure for compactness, although they were advected separately. The flow of the scalar field is well predicted if the flow is aligned parallel to one coordinate direction, such as the cases of (a) and (b) in Fig. 12. However, the prediction becomes somewhat poor for off-axis translation flow, as shown in Fig. 12(c). Interface distortions are mainly shown at the upwind corner of the square [17]. More research is anticipated to make an improvement in the interface tracking algorithm and the momentum advection algorithm as well.

4.5 Mixture theory

In multi-material ALE/Eulerian calculations, eventually a part of the domain is occupied with more than two materials, resulting in a *mixed* cell. It is then necessary to define how the mixed cell partitions the mean strain rate $\dot{\bar{\varepsilon}}$, which is obtained from the Lagrangian step, among the materials. This process is explained by a mixture theory. Once the strain rate of each material is determined, stress of each material is updated to t^{n+1} individually. Finally, the element mean stresses are calculated as the volume-weighted average of the material stresses,

$$\bar{\sigma}^{n+1} = \sum_{m=1}^{N} \left(f^m \sigma_m^{n+1} \right). \tag{33}$$

The simple and robust theory is to partition the mean strain rate of the element to each material, which is called as *equal strain rate* mixture theory.

$$\dot{\bar{\varepsilon}} = \dot{\varepsilon}_1 = \dot{\varepsilon}_2 = \cdots = \dot{\varepsilon}_N . \tag{34}$$

Our numerical experiments reveal that this theory is accurate enough for most high-speed impact problems involving mixed cells filled with materials of no extreme impedance (density × wave speed) mismatch, such as mixtures of solid and solid, or solid and water.

Another scheme is the *pressure equilibrium* mixture theory, which seems to be more versatile for many problems. Each material in a mixed cell is assigned to have different strain rate to allow each material to relax towards pressure equilibrium. It is recommended to adopt an efficient single iteration algorithm, which uses linearized equations of state for each of the *N* materials,

$$P_m^{\,n+1} = P_m^{\,n} - \rho_m c_m^{\,2} \Delta t \dot{\varepsilon}_m^{\,v} , \tag{35}$$

where $\dot{\varepsilon}_m^{\,v}$ is the volume strain rate, ρ_m the density and c_m the wave speed. *N*-1 equations are obtained from Eq. (35). To determine *N* unknowns of $\dot{\varepsilon}_m^{\,v}$, one more constraint equation for the volume strain rate is,

$$\dot{\bar{\varepsilon}}_v = \sum_{m=1}^{N} \left(f^m \dot{\varepsilon}_m^{\,v} \right). \tag{36}$$

This means that the mean volume strain rate is the volume-weighted average of the material volume strain rate. Hence the *N* equations are,

$$P_m^{\,n} - I_m \dot{\varepsilon}_m^{\,v} = P_i^n - I_i \dot{\varepsilon}_i^{\,v} , \text{ for } m = 1, 2, \cdots, N \text{ and } m \neq i \tag{37}$$

$$\dot{\bar{\varepsilon}}_v = f^1 \dot{\varepsilon}_1^{\,v} + f^2 \dot{\varepsilon}_2^{\,v} + \cdots f^{N-1} \dot{\varepsilon}_{M-1}^{\,v} + f^N \dot{\varepsilon}_M^{\,v} , \tag{38}$$

where, $I_i = \rho_i c_i^{\,2} \Delta t$. Here the material of a maximum volume fraction is selected as the pivot material *i*. Solving Eqs. (37) and (38) provides the volume strain rate of the pivot material,

$$\dot{\varepsilon}_i^{\,v} = \frac{\dot{\bar{\varepsilon}}^{\,v} + \sum_{j=1, j\neq i}^{N} \frac{\left(P_i^n - P_j^{\,n} \right)}{I_j} f^j}{f^i + \sum_{j=1, j\neq i}^{N} \frac{I_i}{I_j} f^j} . \tag{39}$$

Then the volume strain rates of all other materials

are obtained by substituting Eq. (39) into Eq. (37). Only this scheme shows no stability problem associated with the mixed cell filled with materials of a huge impedance mismatch. This is the case of the explosions in air.

5. Conclusion

We have devloped a new total shock physics code (ExLO) design to solve large deformation problems involving high-speed impact/penetration and explosions. The program is based on three-dimensional finite element method and written in C++. The distinguishing feature of ExLO is that the Lagrangian, Eulerian and ALE schemes are integrated into a single framework. It can provide an optimum simulation environment for various problems of large deformation problems, such as deep impact/penetration and formation of shaped-charges upon detonation and their subsequent interaction with surrounding targets. Furthermore we can apply the current methodology to FSI problems such that the structural response can be analyzed with Lagrangian scheme while the loading comes from the Eulerian domain.

Benchmark calculations for Taylor bar impact problem show an excellent agreement with previous experimental data. The remap part has been tested with simple analytic velocity fields, in which no stresses are involved. Although a good result is obtained, some improvement is anticipated in the material interface tracking scheme and momentum advection scheme. More practical applications of ExLO to the impact problem and the explosion problem will be described in a separate paper in this journal.

Acknowledgment

Authors greatly acknowledge the support by Defense Acquisition Program Administration and Agency for Defense Development (UD070008AD).

References

[1] J. M. McGlaun, S. L. Thompson and M. G. Elrick, CTH: A three-dimensional shock wave physics code, *Int. J. of Impact Engng.*, 10 (1990) 351-360.

[2] K. G. Budge and J. S. Peery, RHALE: A MMALE Shock Physics Code Written in C++, *Int. J. of Impact Engng.*, 14 (1993) 107-120.

[3] D. J. Benson, A Mixture Theory for Contact in Multi-Material Eulerian Formulations, *Comput. Methods Appl. Mech. Engng.* 140 (1997) 59-86.

[4] M. Lee and Y. H. Yoo, Assessment of a New Dynamic FE-Code: Application to the Impact of a Yawed-Rod Onto Nonstationary Oblique Plate, *Int. J. of Impact Engng.*, 29 (2003) 425-436.

[5] L. B. Tran and H. S. Udaykumar, A particle-level set-based sharp interface cartesian grid method for impact, penetration, and void collapse, *J. Comp. Phys*., 193 (2004) 469-510.

[6] P. D. Bois, Past, Present, and Future of Industrial Crashworthiness Analysis, *Cray Channels*, 12 (1) (1990) 2-5.

[7] T. Belytschko, S. H. Lee, I. S. Yeh, J. I. Lin, C. S. Tsay and J. M. Kennedy, Adaptive in Crashworthiness Calculations, *Shock and Vibration*, 1 (2) (1993) 97-106.

[8] R. M. Summers, S. M. Perry, M. W. Wong, E. S. Hertel, T. G. Trucano and L. C. Chhabildas, Recent progress in ALEGRA development and application to ballistic impacts, *Int. J. of Impact Engng.*, 20 (1997) 779-788.

[9] S. M. Perry and D. E. Carroll, Multi-material ALE methods in unstructured grids, *Comput. Methods Appl. Mech. Engrg.* 187 (2000) 591-619.

[10] M. Lee and W. J. Chung, Development of 3-Dim Simplified ALE Hydrocode: Application to Taylor Impact Test, *Transactions of the KSME (B*), 30 (10) (2006) 1235-1241.

[11] A. Chorin, T. J. R. Hughes, M. F. McCracken and J. E. Marsden, Product formulas and numerical algorithms, *Communications on Pure and Applied Mathematics*, 31 (1978) 205-256.

[12] D. P. Flanagan and T. Belyschko, A Uniform Strain Hexahedron and Quadrilateral and Orthogonal Hourglass Control, *Int. J. Numer. Method Eng*, 17 (1981) 679-706.

[13] K. J. Bathe, Finite Element Procedures. Prentice Hall, Englewood-Cliffs, New Jersey, 1966.

[14] P. J. Madium, J. F. Bingert, J. W. House and S. R. Chen, On the modeling of the taylor cylinder impact test for orthotropic textured materials: Experiments and simulations, *Int. J. of Plasticity*, 15 (1999) 139-166.

[15] W. F. Noh and P. Woodward, SLIC (Simple Line Interface Calculation), Lecture Notes in Physics 59, Springer Verlag (1977).

[16] P. Anninos, New VOF Interface Capturing and Reconstruction Algorithm, Lawrence Livermore National Lab., UCRL-ID-135084, 1999.

[17] M. Rudman, Volume tracking methods for interfacial flow calculations, *Int. J. for Numerical Methods in Fluids*, 24 (1997) 671-691.
[18] D. L. Youngs, An interface tracking method for a 3d eulerian hydrodynamics code, Tech. Report AWRE/44/92/35, AWRE Design Mathematics Division, UK (1987).
[19] D. L. Gueyfher, Li. J. Nadim, R. Scardovelli and S. Zaleski, Volume-of-Interface Tracking with Smoothed Surface Stress Methods for Three-Dimensional Flows, *J. Comp. Phys*., 152 (1999) 423-456.
[20] B. van Leer, Towards the ultimate conservative difference scheme, IV. a new approach to numerical convection, *J. Comp. Phys*., 23 (1997) 276-299.
[21] D. J. Benson, Momentum Advection on a Staggered Mesh, *J. Comp. Phys*., 100 (1992) 143-162.

Appendix

A.1 Taylor impact test with Lagrangian, ALE and Eulerian solvers

The Lagrangian, ALE and Eulerian solvers available in ExLO have been compared for a Taylor impact test using a two-dimensional plain symmetry case. The Eulerian computational domain is 32 × 10 × 1 mesh cells. Initially 30 × 3 × 1 cells are filled with material and the rest is void. The Lagrangian and ALE domains are only 30 × 3 × 1 mesh cells, which is exactly equal to the filled area of the Eulerian model. The impact velocity is 200 *m*/*s*. Material behavior is described by an elastic plastic model with linear hardening. Material density is 8.93 g/cm^3, Young's modulus 100 GPa, Poisson ratio 0.3, initial yield stress 0.4 GPa, and hardening modulus 0.1 GPa. For the option of vertex movement in ALE solution, an equal *x*-distance limitation is enforced to stretch out the grid along the impact direction. Each solution is well comparable, as shown in Fig. A1. Table A1 shows the numerical results for final length and deformed width measured at impact front surface obtained from each solution. The predictions are fairly similar. This benchmark demonstrates the modeling capability as a total shock physics code.

Table A1. Comparison of Taylor impact test, ExLO 2-Dim plain symmetry calculation.

	Lagrangian	ALE	Eulerian
Impact Velocity (m/s)	200		
Initial Length/Initial Width	32 / 3		
Deformed Width (mm)	22.42	23.4	22.1
Final Length (mm)	9.45	9.51	9.55

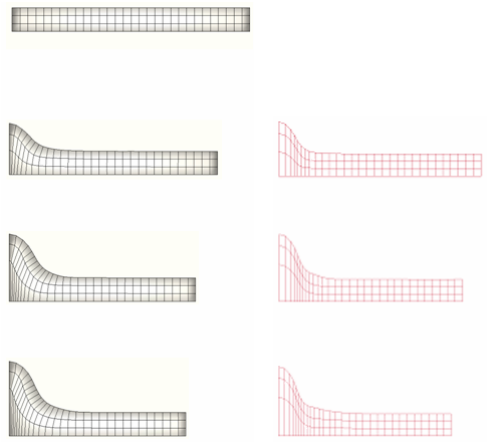

(a) Lagrangian (b) ALE

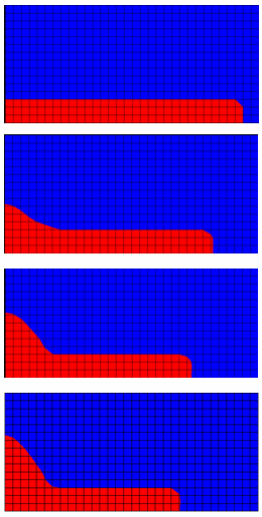

(c) Eulerian

Fig. A1. Two-dimensional plain symmetry Taylor impact test comparison from different schemes.

Minhyung Lee. Professor in the Mechanical and Aerospace Engineering at the Sejong University, Seoul, Korea, holds a PhD from the University of Texas at Austin. His research interests include Lagrangian, Multi-material Eulerian and arbitrary Lagrangian-Eulerian (ALE) finite element methods for high strain rate of large deformation problems (eg, high speed impact/pene-tration, air blast/underwater explosion and bubble dynamics). Prior to joining Sejong University, he was with the US Naval Postgraduate School, Monterey, CA. as a research professor working on the UNDEX problems. He was also with the Institute for Advanced Technol-ogy, Austin, TX. (federated with Army Research Lab.) working on the highly transient dynamics.